Slow light with photorefractive four-wave mixing

Pierre Mathey and Grégory Gadret
Laboratoire Interdisciplinaire Carnot de Bourgogne, UMR 5209 CNRS-Université de Bourgogne, 9 Avenue Alain Savary, Boîte Postale 47870, FR-21078 Dijon Cedex, France

Konstantin Shcherbin*
Institute of Physics, National Academy of Sciences, Prospekt Nauki 46, 03028 Kiev, Ukraine
(Received 14 October 2011; published 1 December 2011)

A slowing down of light pulses using backward-wave four-wave mixing is achieved in photorefractive crystals with different coupling strength. The delay and width of the output pulse are studied as a function of the input pulse width and pump intensity ratio for the amplified transmitted beam and for the phase-conjugated beam. The delay characteristics are compared with those of the two-beam coupling. It is demonstrated that the four-wave mixing process ensures a larger slowing down of short pulses (pulses with width shorter than the photorefractive response time) as compared to the photorefractive two-beam coupling scheme and guarantees the elimination of forerunners. The delay of long pulses in the four-wave mixing configuration is almost the same as the one that can be reached with two-beam coupling. The effect of absorption on the nonlinear shape transformation of the output pulses is discussed qualitatively.

DOI: 10.1103/PhysRevA.84.063802 PACS number(s): 42.65.Hw, 42.70.Nq, 42.81.Dp

I. INTRODUCTION

The term "slow light" denotes a considerable lowering of the group velocity of the light. The propagation of light pulses in a dispersive medium has been studied for more than a century [1,2]. It has been shown by Sommerfeld and Brillouin that the group velocity v_{gr} of light pulses in dispersive media can be smaller or greater than the phase velocity of light $v_{ph} = c/n$ and that it can even become negative. Increased interest in this research field appeared recently when a considerable slowing down of light pulses was achieved using quantum effects of electromagnetically induced transparency (EIT) [3,4]. Since then, slow and fast light have attracted much attention because of the potential applications for highly sensitive interferometry, optical data processing and storage, possible quantum information processing, and control of optical delay lines.

In general, a large dispersion is necessary to achieve a big change of the group velocity. Usually such an additional dispersion is created artificially in different systems using different physical effects. For example, in EIT experiments the dispersion of the probe beam is created when the pump beam is precisely tuned in frequency with respect to the signal for the formation of a certain state in the three-level atom system (Λ system). Slowing down has been achieved with dispersion related to coherent population oscillations [5,6], stimulated Raman scattering [7], and stimulated Brillouin scattering [8], using the dynamic population gratings created by noncollinear [9] or counterpropagating [10] beams, operating in optical fibers [11]. Similarly the strong dispersion of dynamic gratings in the vicinity of Bragg resonance has been used to achieve light pulse deceleration in photorefractive crystals [12,13] and in liquid crystals [14].

The photorefractive techniques operate at room temperature within a wide spectral interval and with no need for precise frequency adjustment of the interacting laser beams. A group velocity down to 0.025 cm/s was achieved with a two-beam coupling scheme [12], when the output signal beam was amplified at the expense of the strong coherent pump beam. Recently it has been shown theoretically [15,16] and demonstrated experimentally [17] that light slowing down can be achieved with photorefractive backward-wave four-wave mixing (BWFWM).

The aim of the present work is a detailed study of slow light realized with BWFWM. This paper has the following structure. In Sec. II the photorefractive two-beam coupling and BWFWM schemes are compared qualitatively for the deceleration of light pulses. Then in Sec. III A the experimental setup is described and some important characteristics of the crystals are estimated. The experimental study of the slow light is presented in Sec. III B. The dependences of the delay of the pulse maximum and the transformation of the pulse width are studied as a function of the input pulse width and the pump intensity ratio in two crystals with different coupling strengths. The results for BWFWM are compared with those obtained for two-beam coupling in the same samples. Then in Sec. IV the experimental data are compared with the theoretical data. The delay characteristics are discussed for different experimental conditions. A possible effect of the absorption on the shape transformation of the delayed pulses is discussed qualitatively.

II. PHOTOREFRACTIVE TWO-BEAM COUPLING AND FOUR-WAVE MIXING FOR SLOWING DOWN OF LIGHT PULSES

We consider a nonlinear medium pumped by two counterpropagating beams I_1 and I_2 as shown in Fig. 1(a). The signal beam I_4 sent to the illuminated region interacts with the pumps giving rise to the appearance of a back-propagating beam I_3. Wave 3 is the phase-conjugate replica of the signal wave 4 for a pair of pump waves (1,2) with mutually conjugated wave fronts [18–20]. This effect is observed in media with

*kshcherb@iop.kiev.ua

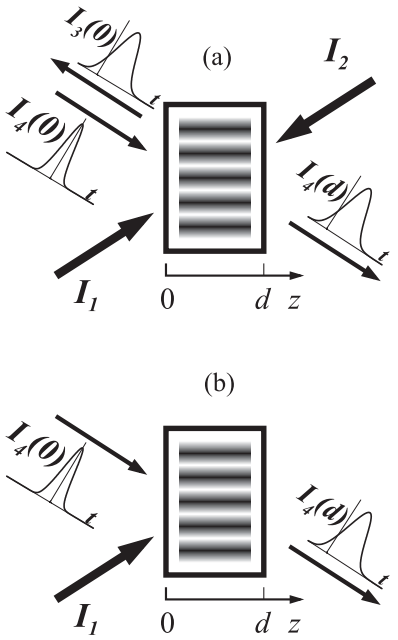

FIG. 1. Schematic representation of the interaction of the beams in BWFWM (a) and two-beam coupling (b) schemes.

different optical nonlinearities and is denoted as backward-wave four-wave mixing. The first experimental realization of BWFWM was reported for Kerr media [20]. Phase conjugation with BWFWM in photorefractive crystals was achieved for continuous-wave [21] as well as for pulsed recording [22].

The spectral response of the photorefractive two-beam coupling [Fig. 1(b)] is determined by the rate coefficient for the wave amplitudes $\Gamma_\omega = \gamma d/(1–i\omega\tau)$, where γ is the coupling constant, which is generally complex, d is the interaction length, and τ is the response time. The coupling constant is real for photorefractive crystals with nonlocal response, where the refractive index grating is $\pm\pi/2$-shifted with respect to the light fringes. In this case the signal beam I_4 bears exponentional amplification because of the energy transfer from the pump I_1: $I_4(\mathrm{d}) = I_4(0)\exp(2\gamma d)$. The real coupling constant gives a Lorentzian frequency response for the two-beam coupling. The spectral profiles of the intensities of the transmitted $I_4(d)$ and phase-conjugated $I_3(0)$ beams in photorefractive BWFWM have a more complicated shape than a Lorentzian one [23] and it also gives rise to dispersion. This dispersion may be used for the slowing down of light pulses.

While a two-beam coupling scheme [Fig. 1(b)] has one output signal $I_4(d)$, BWFWM has two outputs—the transmitted beam $I_4(d)$ and the phase-conjugated beam $I_3(0)$. There is a general difference between these outputs because of their different origin. Similarly to the single output of the two-beam coupling scheme, the transmitted output $I_4(d)$ results from the interference between the part of the input signal $I_4(0)$ transmitted through the crystal and the components diffracted from the pumps in the same direction of $I_4(d)$. If the input pulse is shorter than the photorefractive response time the diffraction efficiency is still far from its steady-state value after the pulse propagation. In this case the uncoupled transmitted signal may dominate in the overall transmitted output. Such a nearly uncoupled transmitted component, which is interpreted in terms of "forerunners" [24], is a serious drawback of the two-beam coupling scheme because it lowers the delay of short pulses nearly to zero. At the same time for short input pulses the diffraction efficiency increases during the whole pulse duration. On the other hand, the backward beam $I_3(0)$ results from diffraction of the pump beams from the grating recorded by the signal and pumps but it does not contain any part of the transmitted signal. Therefore the output conjugated pulse $I_3(0)$ is delayed by a longer interval than the transmitted beam $I_4(d)$ and it is free from the forerunners mentioned above.

III. EXPERIMENT

A. Experimental details and crystal parameters

Either a cerium-doped strontium barium niobate crystal (SBN) or a cobalt-doped barium titanate sample ($BaTiO_3$) are used in the experiment. Two continuous-wave (cw) counterpropagating pump beams I_1 and I_2 from an Ar^+ laser ($\lambda = 514$ nm) enter the sample as shown in Fig. 1(a). A weak signal beam $I_4(0)$ with an intensity of the order of 10^{-5} of the total pump intensity impinges on the sample at an angle of $2\theta \approx 20^\circ$ with respect to the pump I_1 (grating spacing $\Lambda \approx 1.4\ \mu$m). All the beams are polarized in the plane of incidence. The path difference between the three incident beams is chosen so that the beam I_2 is not coherent to the two mutually coherent beams I_1 and I_4. This ensures that only a transmission grating is recorded. Both crystals have their edges parallel to the crystal axes. The SBN crystal is placed in such a way that its c axis is parallel to the grating vector and its input face is nearly perpendicular to the bisector of the angle between beams I_1 and I_4. The c axis of the $BaTiO_3$ sample is perpendicular to the input face and lies in the plane of incidence. The input face of the $BaTiO_3$ is tilted by nearly 45° in the plane of incidence to get the benefit of the largest component r_{42} of the electro-optic tensor of $BaTiO_3$ [25]. The $\pi/2$-shifted grating recorded in the crystals in the diffusion regime leads to an energy coupling between the beams I_1 and I_4. The crystals are oriented in such a way that the transmitted beam $I_4(d)$ is amplified while the phase-conjugated beam $I_3(0)$ is attenuated.

In the experiments the Gaussian temporal profile of the input pulse is shaped by an electro-optic modulator, with intensity $I_4(d = 0,t) = I_4^0 \exp(-t^2/t_0^2)$, where t_0 is the $1/e$ half-width of the pulse intensity. The temporal envelopes of the input $I_4(0,t)$, transmitted $I_4(d,t)$, and phase-conjugated $I_3(0,t)$ signals are recorded for different experimental conditions.

For the evaluation of the coupling strengths of our crystals the phase-conjugate reflectivity is measured with the cw beam $I_4(0)$ as a function of the pump ratio $r = I_2(d)/I_1(0)$. The experimental data are shown by squares for the SBN crystal in Fig. 2(a) and for $BaTiO_3$ in Fig. 2(b). The phase-conjugate reflectivity R_{pc} depends on the pump beam ratio as [20]

$$R_{pc} = \frac{I_3(0)}{I_4(0)} = r\left|\frac{1-\exp(\gamma d)}{1+r\exp(\gamma d)}\right|^2. \qquad (1)$$

The solid lines in Fig. 2 are a best fit of Eq. (1) to the experimental data. The coupling strengths deduced from the optimal pump ratio are $\gamma d = \ln(r_{\mathrm{opt}}) = \ln(0.18) \approx -1.7$ for the SBN crystal and $\gamma d = \ln(0.06) \approx -2.8$ for the $BaTiO_3$

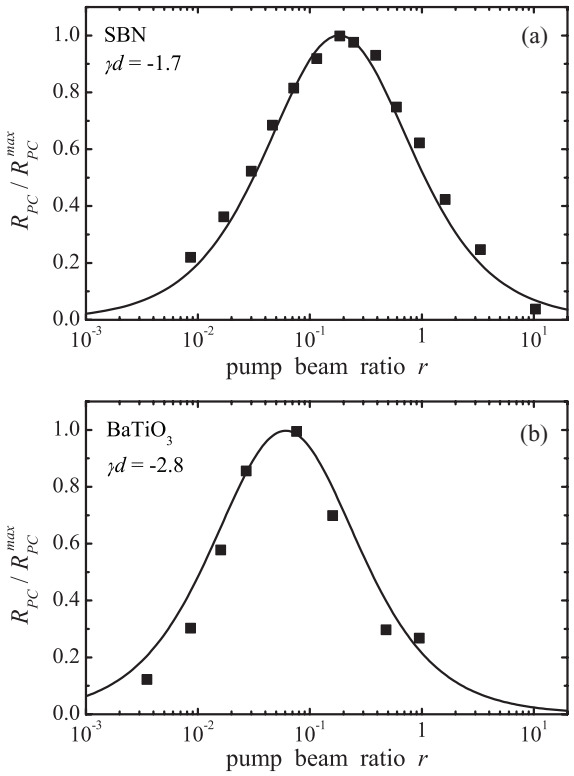

FIG. 2. Normalized phase-conjugate reflectivity $R_{pc}/R_{pc}^{\max}$ as a function of the pump ratio r for (a) SBN and (b) $BaTiO_3$ crystal; squares: experimental data; solid lines: best fit of Eq. (1).

crystal. The response time evaluated from the two-beam coupling grating formation time is $\tau = 1.4$ s for the SBN crystal and $\tau = 0.8$ s for the $BaTiO_3$ crystal. At the recording wavelength $\lambda = 514$ nm the absorbance is estimated to be $\alpha d \approx 0.5$ for the SBN crystal and $\alpha d \approx 0.4$ for the $BaTiO_3$ sample.

B. Experimental results

The temporal envelopes of the input $I_4(0,t)$, transmitted $I_4(d,t)$, and phase-conjugated $I_3(0,t)$ signals are recorded for input pulses with different half-widths and for a pump ratio close to the optimal one, i.e., $r = 0.18$ for the SBN crystal and $r = 0.076$ for the $BaTiO_3$ sample. The temporal dependences for the SBN crystal for input pulses with half-widths $t_0 = 0.16$s, $t_0 = 0.44$ s, and $t_0 = 1.6$ s are presented in Figs. 3(a)–3(c), respectively (the input pulses are shown by thin lines). The transmitted beam $I_4(d,t)$ for the shortest input [Fig. 3(a)] consists of a pulse that is nearly unshifted in time and with a slow-decaying tail. The tail corresponds to the diffraction decay of the pump I_1 from the grating recorded during the pulse duration. The uncoupled transmitted component dominates in the output signal $I_4(d,t)$ over the relatively small diffracted component. This is why the maximum of the transmitted pulse is nearly not delayed. At the same time the maximum of the phase-conjugated beam $I_3(0,t)$ is delayed by nearly the whole input pulse duration. For a longer input pulse ($t_0 = 0.44$ s) the delay of the transmitted pulse slightly increases [Fig. 3(b)], its tail becomes more pronounced, but the deceleration of the phase-conjugated pulse is much larger. For the input width $t_0 = 1.6$ s the shapes of both outputs become similar

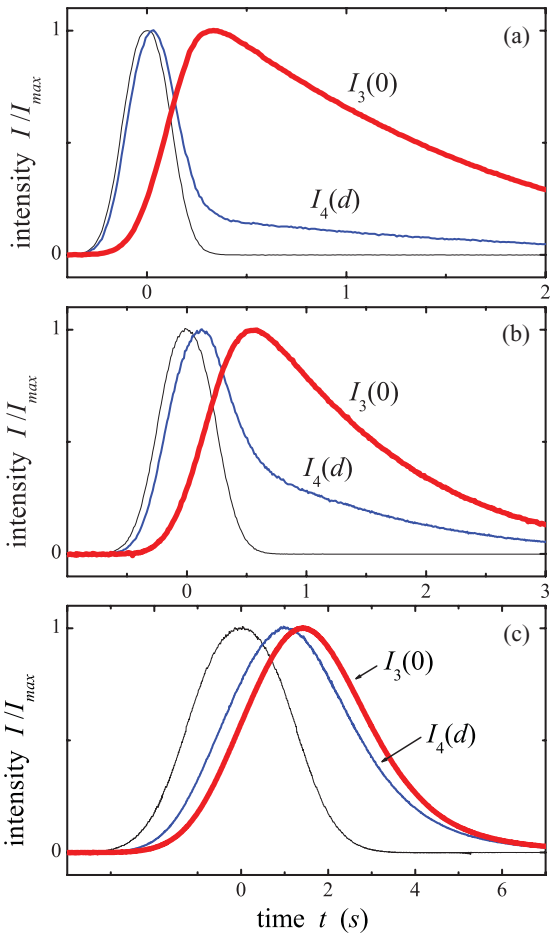

FIG. 3. (Color online) Temporal variation of the intensities of input pulse $I_4(0)$ (thin lines), transmitted $I_4(d)$, and phase-conjugated $I_3(0)$ pulses for the SBN crystal with input pulse half-width (a) $t_0 = 0.16$ s, (b) $t_0 = 0.44$ s, and (c) $t_0 = 1.6$ s.

[Fig. 3(c)], because the diffractive contribution dominates in the transmitted beam $I_4(d,t)$. Nevertheless the conjugated beam $I_3(0,t)$ is still delayed for a longer time. With a further increase of the input pulse width the delay and the shape of both pulses become nearly identical.

The situation changes dramatically if a crystal (like $BaTiO_3$) with a larger coupling constant is used. At the beginning the temporal envelope of the transmitted beam $I_4(d,t)$ nearly retraces the short input pulse $I_4(0,t)$ with $t_0 = 44$ ms, as shown in Fig. 4(a), but then the tail observed with the SBN crystal is substituted by a long pulse with an amplitude much smaller than the amplitude of the first short pulse. The temporal behavior of the conjugated beam $I_3(0,t)$ is also different: A relatively slow growth of the intensity is observed after the input pulse propagation for the larger coupling constant of the $BaTiO_3$ crystal [Fig. 4(a)] instead of a slow decay in the case of SBN [Fig. 3(a)]. The amplitude of the second broad pulse in the transmitted beam $I_4(d,t)$ becomes larger for a longer input, as shown in Fig. 4(b) for $t_0 = 0.16$ s, and it even overcomes the first peak for an input width $t_0 = 0.22$ s [see Fig. 4(c)]. Then the first peak, which is related to a nearly uncoupled transmitted component of the input pulse, disappears as is shown in Fig. 4(d) for $t_0 = 0.44$ s, because

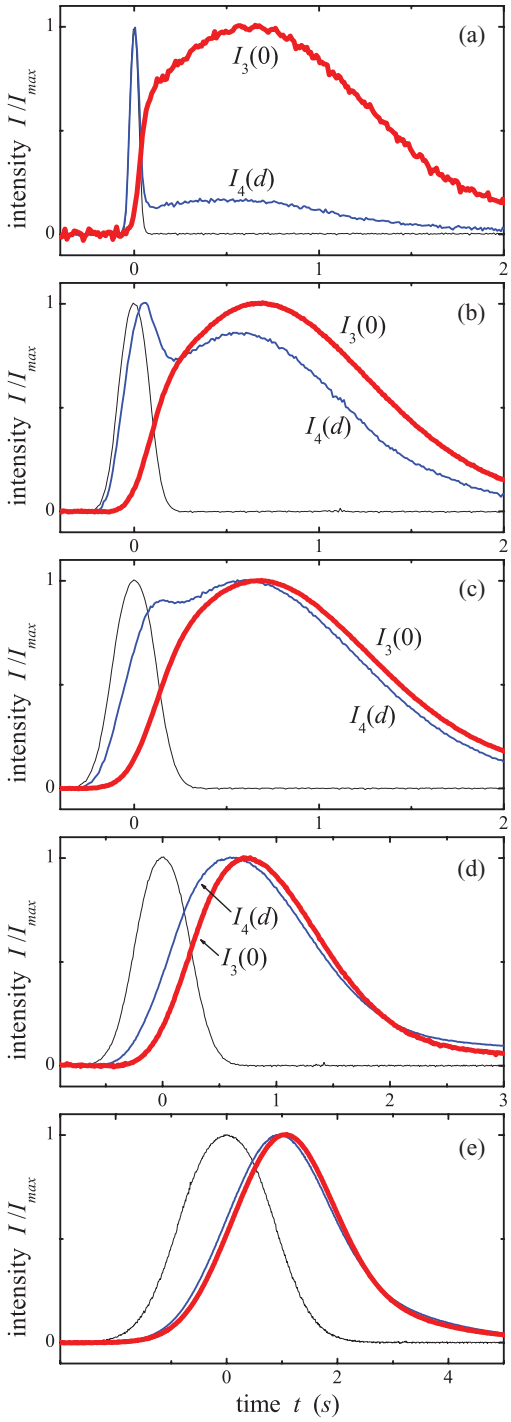

FIG. 4. (Color online) Temporal variation of the intensities of input pulse $I_4(0)$ (thin lines), transmitted $I_4(d)$, and phase-conjugated $I_3(0)$ pulses for the $BaTiO_3$ crystal with input pulse half-width (a) $t_0 = 44$ ms, (b) $t_0 = 0.16$ s, (c) $t_0 = 0.22$ s, (d) $t_0 = 0.44$ s, (e) $t_0 = 1.6$ s.

this component is covered by the second strongly amplified maximum (diffractive component). For all the inputs within this range the conjugated beam $I_3(0,t)$ always consists of one pulse with a maximum delayed for an interval that is longer than the single or both maxima of the transmitted beam $I_4(d,t)$. The temporal behavior of the transmitted and phase-conjugated outputs becomes nearly identical for longer input pulses, as is shown in Fig. 4(e) for $t_0 = 1.6$ s.

For the characterization of the slowing down of the light pulses we use a time interval Δt between the maximum of the input pulse intensity and the maximum of the output pulse $I_3(0,t)$ or $I_4(d,t)$. For the evaluation of the transformation of the output pulses we use the output pulse half-width w at the intensity level $1/e$ normalized to the input pulse half-width t_0. In the case of two maxima in the transmitted beam $I_4(d,t)$ the absolute (i.e., the largest) maximum is considered as a maximum of the whole output pulse and the half-width is measured for the full output.

The output characteristics for the SBN crystal with $r = 0.18$ are shown in Fig. 5. The delay of the output pulses as a function of the input pulse half-width t_0 are shown in Fig. 5(a) while the normalized output pulse half-width is plotted in Fig. 5(b) by filled squares for the conjugated beam $I_3(0)$ and by open diamonds for the transmitted beam $I_4(d)$. It is obvious that the conjugated beam is delayed by more than one order of magnitude compared to the transmitted beam for the short input pulses. The duration of the transmitted beam is nearly unchanged ($w/t_0 \approx 1$) for short inputs because the pulse is transmitted with nearly no coupling. On the contrary the un-normalized width of the phase-conjugated beam w is nearly constant for the short inputs and it almost does not depend on the input pulse duration [w/t_0 decreases $\sim t_0^{-1}$ for the normalized signal as is presented in Fig. 5(b)]. The shape of both outputs approaches the shape of the input beam for long pulses when the grating follows the input pulse, i.e., when the input pulse matches the bandwidth of the Bragg resonance. It should be noted that the dependences in Fig. 5

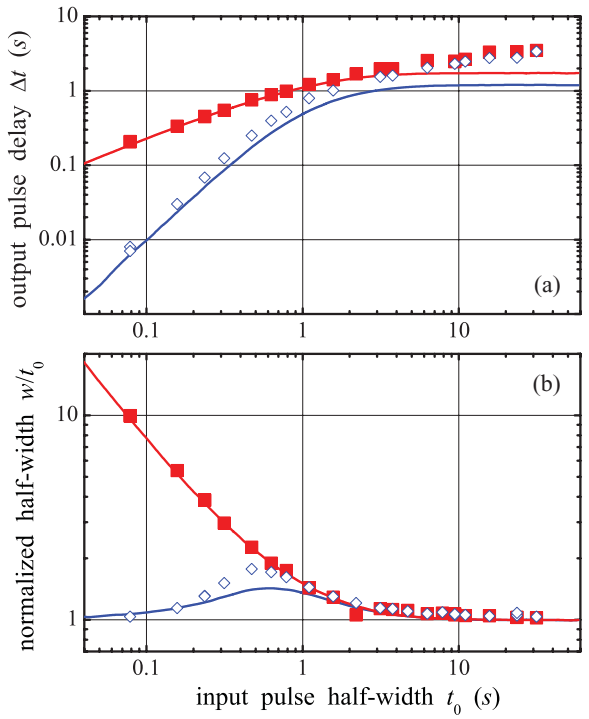

FIG. 5. (Color online) SBN crystal, $r = 0.18$; (a) delay of output pulse maxima and (b) normalized output pulse half-width as a function of the input pulse half-width for transmitted $I_4(d)$ (diamonds) and phase-conjugated $I_3(0)$ (squares) beams; solid lines: theoretical calculations.

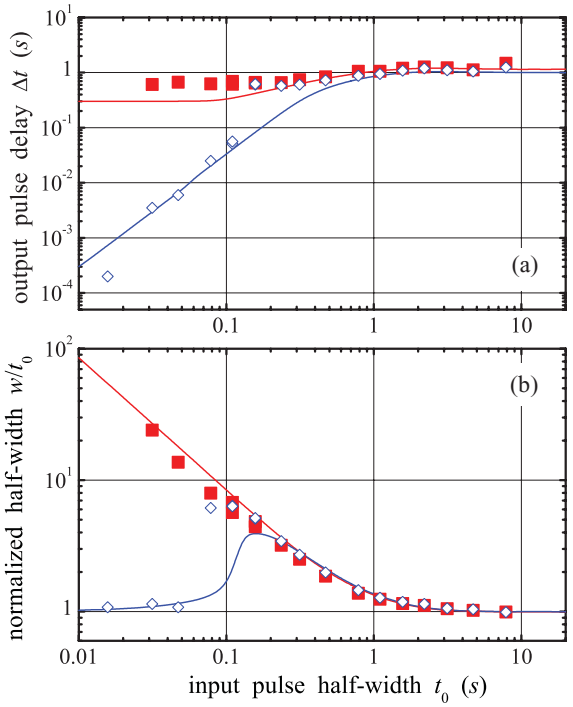

FIG. 6. (Color online) $BaTiO_3$ crystal, $r = 0.076$; (a) delay of output pulse maxima and (b) normalized output pulse half-width as a function of the input pulse half-width for transmitted $I_4(d)$ (diamonds) and phase-conjugated $I_3(0)$ (squares) beams; solid lines: theoretical calculations.

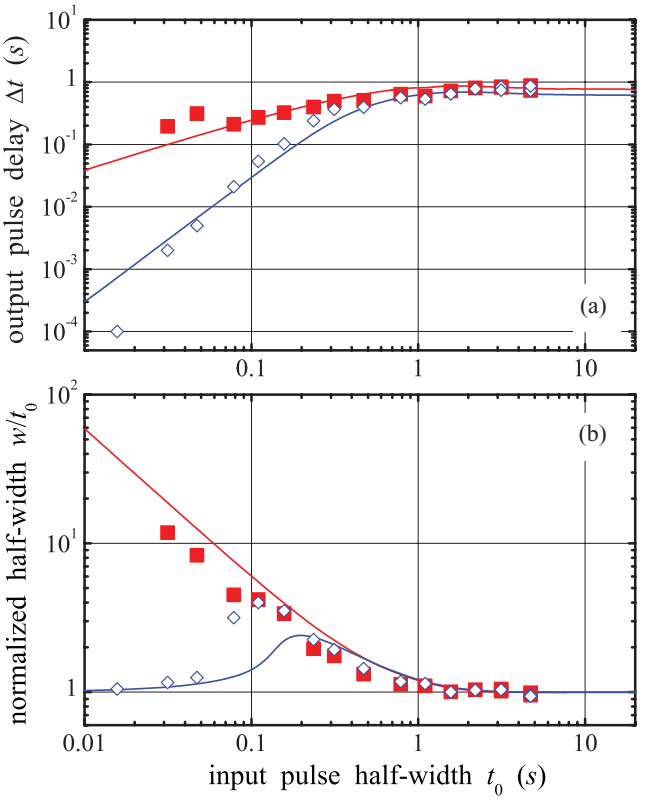

FIG. 7. (Color online) $BaTiO_3$ crystal, $r = 0.16$; (a) delay of output pulse maxima and (b) normalized output pulse half-width as a function of the input pulse half-width for transmitted $I_4(d)$ (diamonds) and phase-conjugated $I_3(0)$ (squares) beams; solid lines: theoretical calculations.

for the transmitted beam $I_4(d)$ bear a close analogy with the dependences for a pulse slowing down in the two-beam coupling scheme reported earlier [12].

Dependences similar to that presented in Fig. 5 for the SBN sample but characterizing the slowing down of light pulses in the $BaTiO_3$ crystal are presented in Fig. 6 for $r = 0.076$. The delay of short pulses is nearly constant for the conjugated beam $I_3(0)$ and it exceeds the delay of the transmitted beam $I_4(d)$ even more than in the case of the SBN crystal that has a smaller coupling constant. The dependences of the delay and half-width for the transmitted beam are smooth for the SBN crystal while a jump is observed in the corresponding dependences for the $BaTiO_3$ crystal. This jump is related to the second maximum appearing in the transmitted beam $I_4(d,t)$. Obviously the delay of the transmitted beam maximum increases with a jump when the amplitude of the second maximum becomes larger than the amplitude of the first one. Similarly, the half-width of the transmitted output increases with a jump when the intensity of the second maximum reaches the $1/e$ level of the absolute maximum of the transmitted beam. The amplitude of the jump and its position in the interval of the input pulse width depend on the method of estimation of the output pulse parameters. However, such a jump should be observed for the transmitted beam with a different determination of the delay and width of the output pulses.

Compared to the two-beam coupling technique the additional control parameter of the BWFWM scheme is the pump beam ratio r. We study now how this ratio acts on the output pulse characteristics. This study has been conducted for both crystals but in the following we choose to present the results for the most rich and interesting case of the $BaTiO_3$ sample that has the highest coupling constant. The experimentally measured delay of the output pulses and their normalized half-width as a function of the input pulse width measured with $r = 0.16$ are plotted in Fig. 7 by dots. The delay of both output pulses and their nonlinear shape transformation become smaller compared to the dependences shown in Fig. 6 for $r = 0.076$. The dependences for the transmitted beam $I_4(d)$ become smooth with no jump similarly to the dependences in Fig. 5 for the SBN crystal because the second peak in the temporal envelope $I_4(d,t)$ is not so pronounced for this beam ratio and it is observed in a narrower interval of t_0.

For better understanding of the effect of the pump beam ratio on the delay characteristics we present in Fig. 8 the delay of maxima for both outputs as a function of the beam ratio for input pulses with different durations. The experimental data for the transmitted beam $I_4(d)$ are shown by open diamonds and by solid squares for the conjugated output $I_3(0)$. As for all previous data related with short pulses the delay of the conjugated beam is more than one order of magnitude larger as compared to the delay of the transmitted beam, in the whole range of the pump beam ratio, as illustrated in Fig 8(a) for the input width $t_0 = 44$ ms. This difference becomes smaller for a longer input width $t_0 = 0.11$ s [Fig. 8(b)]. For an input

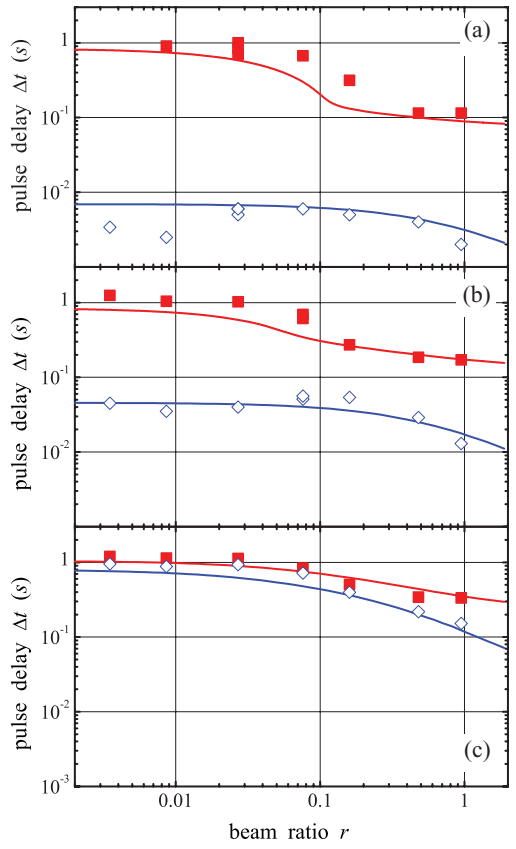

FIG. 8. (Color online) Delay of output pulse maxima as a function of the pump ratio in $BaTiO_3$ crystal for transmitted $I_4(d)$ (diamonds) and phase-conjugated $I_3(0)$ (squares) beams with input pulse half-width (a) $t_0 = 44$ ms, (b) $t_0 = 0.11$ s, and (c) $t_0 = 0.44$ s; solid lines: theoretical calculations.

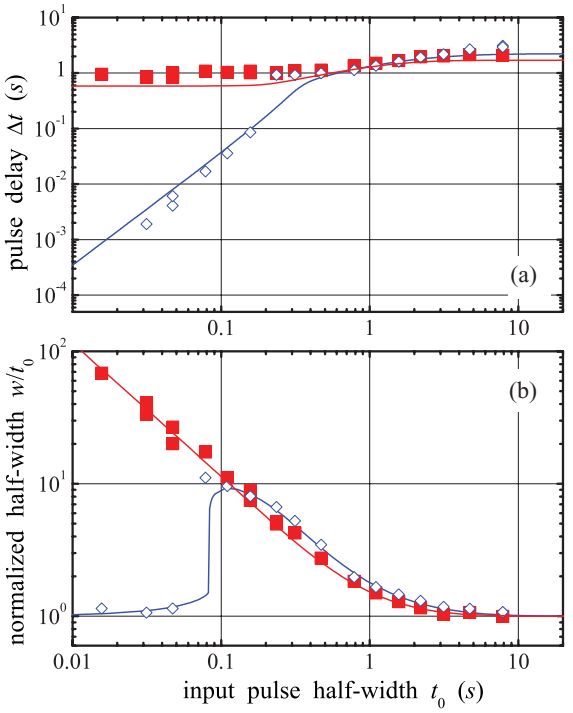

FIG. 9. (Color online) (a) Delay of output pulse maxima and (b) normalized output pulse half-width as a function of the input pulse half-width for transmitted beam in two-beam coupling experiment $I_4(d)$ (diamonds) and phase-conjugated beam $I_3(0)$ in BWFWM with $r = 0.027$ (squares) beams in $BaTiO_3$; solid lines: theoretical calculations.

pulse whose half-width is $t_0 = 0.44$ s, i.e., that becomes comparable with the response time of the crystal ($\tau = 0.8$ s) the dependences of the delay for both output pulses converge for small beam ratios [see Fig. 8(c)]. The delay slightly increases for both output pulses with a further increase of the input pulse duration and the dependences converge in the whole studied interval of the beam ratios.

As follows from the plots in Fig. 8 the delay of both outputs increases with the decreasing of the beam ratio and it tends to saturate at the smallest beam ratio. The BWFWM with a pump ratio r equal to zero is nothing else than the two-beam coupling configuration. In this case there is no conjugated beam $I_3(0)$ because there is no pump I_2 to diffract backward the input signal $I_4(0)$, only the transmitted output $I_4(d)$ exists. Therefore, for the transmitted output, the largest delay is expected to be obtained for $r = 0$. This delay can be compared with the delay of the conjugated beam at a certain small beam ratio. We conduct this comparison of the slowing down of the light pulses in the two-beam coupling and in BWFWM configurations. The delay of the transmitted beam as a function of the input pulse half-width measured in the two-beam coupling scheme with the $BaTiO_3$ crystal is shown in Fig. 9(a) by open diamonds. The corresponding pulse shape transformation is shown in Fig 9(b). The delay characteristics of the conjugated beam $I_3(0)$ measured in the BWFWM configuration with $r = 0.027$, which is only slightly shifted from the optimal beam ratio $r_{opt} \approx 0.06$, are shown in the same Fig. 9 by filled squares together with the data for the two-beam coupling. It is evident that the delay of the short pulses achieved with BWFWM is much larger as compared with the two-beam coupling scheme. For long pulses the delay of the conjugated beam $I_3(0)$ is almost the same as that measured for the transmitted beam $I_4(d)$ in the two-beam coupling geometry.

Finally we present in Fig. 10 the maximum intensity for the transmitted and conjugated pulses as a function of the input pulse half-width for the optimal beam ratio $r = 0.076$. The maximum of the transmitted pulse $I_4^{max}(d)$ in Fig. 10(a) is normalized by the maximum intensity of the signal behind the crystal with no pump $I_4^0(d)$. Short pulses propagate through the crystal with nearly no change. The transmitted intensity increases rapidly for longer pulses and reaches its saturated value for input pulses with half-width slightly overcoming the crystal response time. The conjugated beam intensity dependence drawn in Fig. 10(b) is corrected for losses in the crystal of both impinging signal and emerging conjugated beam, i.e., the measured intensity is multiplied by $\exp(2\alpha d)k_0^2$, where k_0 is a reflection coefficient. The maximum intensity of the conjugated pulse increases quadratically for the short inputs as shown in Fig. 10(b) and saturates also at a half-width value of the input pulse that is slightly larger than the crystal response time, i.e., when the signal matches the bandwidth of the Bragg resonance.

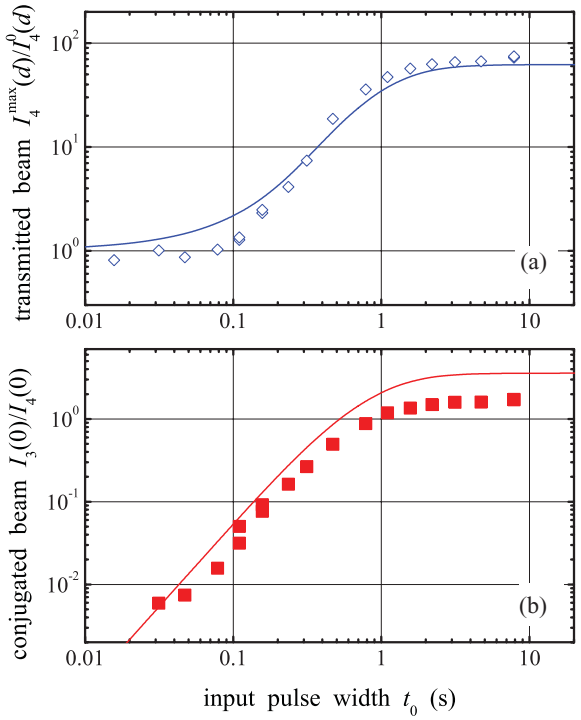

FIG. 10. (Color online) Maximum intensity for the (a) transmitted and (b) conjugated pulses as a function of the input pulse half-width for $BaTiO_3$ with $r = 0.076$. Experimental data for the conjugated beam are corrected for losses (see text for details).

IV. DISCUSSION

A. Comparison with theory

According to the theory the Fourier components of the amplitudes of the conjugated $\tilde{A}_3^*(0,\omega)$ and transmitted $\tilde{A}_4(d,\omega)$ output waves can be expressed via the Fourier component of the input signal $\tilde{A}_4(0,\omega)$ as [16]

$$\tilde{A}_3^*(0,\omega) = \sqrt{r}\exp(-i\varphi)\frac{1-\exp(\Gamma_\omega d)}{1+r\exp(\Gamma_\omega d)}\tilde{A}_4(0,\omega), \quad (2)$$

$$\tilde{A}_4(d,\omega) = \frac{(1+r)\exp(\Gamma_\omega d)}{1+r\exp(\Gamma_\omega d)}\tilde{A}_4(0,\omega), \quad (3)$$

where $\varphi = \arg(A_1A_2)$ is a constant phase and the asterisk indicates complex conjugation. For a Gaussian-shaped input amplitude $A_4(0,t) = A_4^0\exp(-t^2/2t_0^2)$, which we use in the experiment, the Fourier transform is $\tilde{A}_4(0,\omega) = (A_4^0 t_0/\sqrt{2\pi})\exp(-\omega^2 t_0^2/2)$. The output intensities $I_3(0,t) = |A_3(0,t)|^2$ and $I_4(d,t) = |A_4(d,t)|^2$ can be calculated from Eqs. (2) and (3) using the inverse Fourier transform. Then the delay of the pulse maximum Δt, the half-width w at the intensity level $1/e$, and the intensity maxima $I_3^{max}(0)$, $I_4^{max}(d)$ can be evaluated for both output pulses from the temporal envelopes of their intensities. The solid lines in Figs. 5–10 represent the corresponding theoretical calculations of the characteristics of both delayed pulses using Eqs. (2) and (3). It should be noted that the calculations are performed with the independently evaluated values of the coupling constant and response time, presented in Sec. II A, with the given intensity ratio r but with no fitting parameters.

B. Discussion of the experimental results

It clearly appears from the temporal profiles of the outputs for both crystals shown in Figs. 3 and 4 that for short input pulses with half-width t_0 smaller than the response time of the crystal τ the backward pulse $I_3(0)$ is delayed for a longer time than the pulse of the transmitted beam $I_4(d)$. The light-induced index grating is at its initial stage of development and far from the steady state. This is why the uncoupled transmitted component dominates in the output signal $I_4(d,t)$ over the relatively small diffracted component. As a result the maximum of the transmitted pulse is nearly not delayed. At the same time the maximum of the backward beam $I_3(0,t)$ is delayed by nearly the total duration of the input pulse for the SBN crystal [Fig. 3(a)]. It is delayed even longer for $BaTiO_3$ because of its larger coupling constant [Figs. 4(a)) and 4(b)].

For short inputs the difference in the pulse delay for the conjugate and transmitted outputs exceeds one order of magnitude as illustrated in Figs. 5(a) and 6(a). In fact, such a dramatic difference is observed for pulses with spectral content beyond the bandwidth of the system, i.e., for input pulses with a half-width much shorter than the photorefractive response time. The decaying tail of the conjugate output $I_4(d,t)$ corresponds to the crystal response time and therefore it is much longer than the leading edge. This is why the large delay of the short pulses with phase conjugation does not allow an operation at high frequency corresponding to the input pulse width because of the relatively slow pulse decay. At the same time, for signal processing operation, the rise of a wanted signal to a certain level is important. Most of the electronic components operate with signal edges. The fast delayed leading edge of the conjugate output can be used in a similar way for signal processing in systems that do not require a high repetition rate.

For long enough input pulses that match the bandwidth of the system the absolute value of the delay increases and reaches its maximal value, which is almost identical for both outputs [see Figs. 5(a) and 6(a)]. A question may arise whether the delay in the BWFWM configuration is comparable to that achieved with two-beam coupling. Indeed, if we consider the recording of transmitting gratings only by beams I_1 and I_4, as is done in our BWFWM experiment, the counterpropagating pump I_2 acts in part as an erasing beam reducing the contrast of the light fringes and decreasing somewhat the direct coupling of beams I_4 and I_1. That is why the coupling of the transmitted output in BWFWM scheme is always reduced as compared to the two-beam coupling where I_2 is absent. Therefore for the pulses that match the bandwidth of the crystal the larger delay is expected in the two-beam coupling scheme. This is confirmed by the experimental dependences of the delay as a function of the beam ratio shown in Fig. 8: The smaller r is, the larger the delay. At the same time the direct comparison presented in Fig. 9 clearly demonstrates that BWFWM in the $BaTiO_3$ crystal with a small $r = 0.027$ ensures almost the same delay of long pulses as the two-beam coupling scheme. Of course it is natural to operate in BWFWM at an optimal beam ratio. It should be noted here that the optimal beam ratio is quite small for large coupling strength $r_{opt} = \exp(\gamma d)$, which is negative for our crystal orientation. So, the BWFWM configuration with crystals that possess a large coupling

strength ensures at an optimal beam ratio almost the largest possible pulse delay.

A difference in the temporal envelopes of both transmitted and conjugated signals is observed for the BWFWM in crystals with different coupling constants (see Figs. 3 and 4). With a small coupling constant the outputs always decay after the input pulse propagation (SBN) while with a greater coupling strength ($BaTiO_3$) the intensity increases after the propagation of a short pulse for both the transmitted $I_4(d,t)$ and the conjugate $I_3(0,t)$ beam. Such a transient intensity growth is referred to as self-enhancement (see, e.g., [26]) and can be explained for two-beam coupling as follows. The grating is not erased immediately after the recording with a short pulse. The pump I_1 diffracted from the slow decaying grating produces a seeding beam. This seeding beam is amplified all along its propagation in the crystal from the input face to the output face because of the direct energy transfer from the pump I_1. As a result, the fringe contrast increases with the crystal depth. At the initial stage of this self-enhancement process and with a large coupling constant, the overall increase of the contrast overcomes the natural grating erasure. Then, with no input signal, the dynamic grating moves from the input to the output face of the crystal and finally disappears. In such a way the second maximum appears in the transmitted $I_4(d,t)$. The conditions for the existence of two maxima in the temporal profile of the transmitted beam $I_4(d,t)$ have been analyzed for two-beam coupling [27]. In the case of BWFWM the situation is more complicated: Two self-developing dynamic gratings move towards each other in the direction of the opposite crystal faces. Even a mirrorless oscillation can appear if threshold conditions are fulfilled [19]. Below the threshold, however, the physics of the self-enhancement in photorefractive BWFWM is similar to that in the two-beam coupling scheme. Thus, the specific temporal profiles of the transmitted beam with two maxima observed for short input pulses in the crystal with the larger coupling constant ($BaTiO_3$) can be explained by a pronounced self-enhancement effect.

C. Effect of absorption

Qualitatively the theoretical calculations [16] describe well most of the experimental data. However, the theory does not explain some peculiarities of the experimental dependences such as the sharp jumps of the delay for the transmitted pulse $I_4(d)$ [open diamonds in Figs. 6(a) and 9(a)] and its jumplike shape transformation [open diamonds in Fig. 6(b)] in the dependences on the input pulse width. Such jumplike features arise when the second maximum becomes important for the evaluation of the delay and width of the output pulses. Thus, the theory under the undepleted pump approximation [16] predicts a not-so-pronounced second maximum in the temporal envelope of the transmitted beam $I_4(d,t)$ or sometimes even the absence of two maxima at all. The larger nonlinear distortion of the output signals, which is observed in the experiment, can be interpreted in terms of a transformation of the system bandwidth.

It is known that the bandwidth of the two-beam coupling gain exhibits a transformation in the case of nonuniform intensity distribution in the crystal bulk [28], because the photorefractive response is inversely proportional to the intensity. The nonuniformity of the intensity along the z axis is caused by the linear absorption. The nonuniformity in the direction perpendicular to z arises when the grating is recorded with unexpanded beams of Gaussian intensity distribution. In what follows we analyze the bandwidth of a Bragg resonance in the presence of absorption for the two-beam coupling scheme because a simple analytical solution can be found in this case for the corresponding transformation of dispersion and group velocity. Analogous changes of the transmittance, nonlinear phase shift, and group velocity spectra for the transmitted wave A_4 in BWFWM have the same origin and therefore BWFWM exhibits a similarity with the two-beam coupling.

As the photorefractive response time is inversely proportional to the light intensity, the position-dependent time constant is given by $\tau(z) = \tau_0 I_0/I(z) = \tau_0 \exp(\alpha z)$, where τ_0 and I_0 are the response time and intensity on the input face of the crystal. In the case of two-beam coupling with a nonlocal response the variation of the signal along the z axis is

$$\begin{aligned} A_4(z,\omega) &= A_4^0 \exp\left(-\frac{\alpha z}{2} + \Gamma_\omega z\right) \\ &= A_4^0 \exp\left[-\frac{\alpha z}{2} + \gamma'(\omega) z + i\gamma''(\omega) z\right], \end{aligned} \tag{4}$$

where

$$\begin{aligned} \gamma'(\omega) &= \gamma_0/[1+\omega^2\tau^2(z)], \\ \gamma''(\omega) &= \gamma_0\omega\tau(z)/[1+\omega^2\tau^2(z)] \end{aligned} \tag{5}$$

are the real and imaginary parts of the complex amplitude gain $\gamma(\omega) = \gamma'(\omega) + i\gamma''(\omega)$ and γ_0 is the steady-state coupling constant for wave amplitudes. The real part of the gain is responsible for the energy transfer while the imaginary part determines the nonlinear phase change of the output wave. The spectra of the integral coupling constants with a decaying intensity in an absorbing crystal are given by

$$\gamma'(\omega) = \frac{1}{d}\int_0^d \frac{\gamma_0}{1+\omega^2\tau^2(z)} dz, \tag{6}$$

$$\gamma''(\omega) = \frac{1}{d}\int_0^d \frac{\gamma_0\omega\tau(z)}{1+\omega^2\tau^2(z)} dz. \tag{7}$$

The integration with substitution of $\tau(z)$ gives the expressions for the spectra of the coupling constants:

$$\gamma'(\omega) = \gamma_0\left\{1 + \frac{1}{2\alpha d}\ln\left[\frac{1+\omega^2\tau_0^2}{1+\omega^2\tau_0^2\exp(2\alpha d)}\right]\right\}, \tag{8}$$

$$\gamma''(\omega) = \frac{\gamma_0}{\alpha d}\{\arctan[\omega\tau_0\exp(\alpha d)] - \arctan(\omega\tau_0)\}. \tag{9}$$

The nonlinear phase shift of the signal wave $A_4(d)$, which determines the slowing down of the group velocity with photorefractive two-beam coupling, is characterized by γ''. The spectrum of the group velocity, which is due to this nonlinear phase shift, may be expressed as [29]

$$v_{gr}(\omega) = \frac{c}{n + c\frac{d\gamma''(\omega)}{d\omega}}, \tag{10}$$

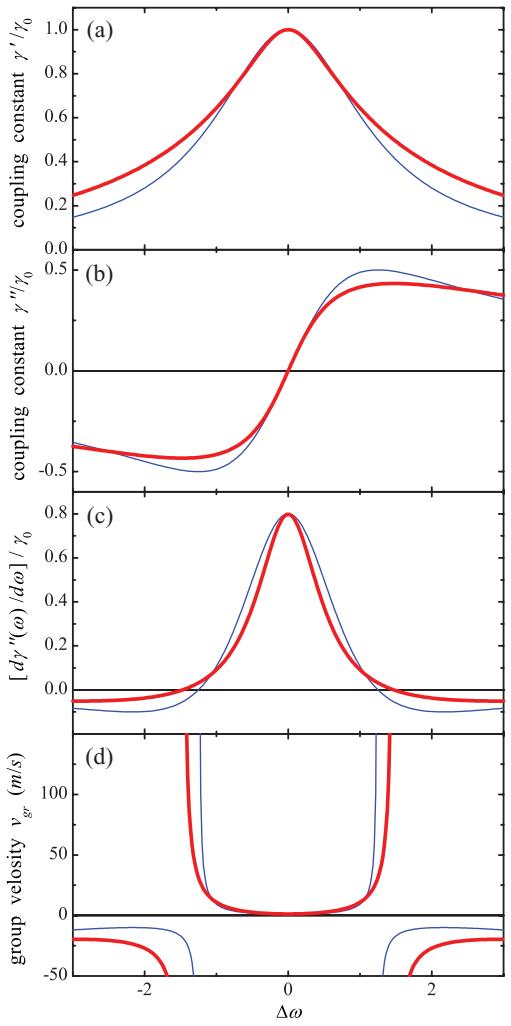

FIG. 11. (Color online) Spectra of the (a) real and (b) imaginary parts of the coupling constant, (c) of the slope $[d\gamma''(\omega)/d\omega]/\gamma_0$, and (d) group velocity calculated for two-beam coupling with $\tau = 0.8$ s for zero absorption (thin lines) and for $\alpha d = 2$ (thick lines).

where n is the averaged refractive index of the medium, c is the light speed in vacuum, and the slope $d\gamma''(\omega)/d\omega$ is given by differentiating Eq. (9):

$$\frac{d\gamma''(\omega)}{d\omega} = \frac{\gamma_0\tau_0}{\alpha d}\left[\frac{\exp(\alpha d)}{1+\omega^2\tau_0^2\exp(2\alpha d)} - \frac{1}{1+\omega^2\tau_0^2}\right]. \quad (11)$$

The thin lines in Fig. 11 represent the calculated spectra for zero absorption and with $\tau(z) = \text{const.} = 0.8$ s. The spectrum of the normalized coupling constant for wave amplitudes $\gamma'(\omega)/\gamma_0$ is plotted in Fig. 11(a). Figure 11(b) shows the relative change of the phase coupling constant $\gamma''(\omega)/\gamma_0$. The derivative of $[d\gamma''(\omega)/d\omega]/\gamma_0$ calculated analytically from Eq. (5) is plotted in Fig. 11(c) and the resulting group velocity spectrum is represented in Fig. 11(d).

A correct comparison of the bandwidths with different values of the absorption should be conducted for the same integral response time constants, but not for equal time constants at the input face $\tau_0 = \tau(z = 0)$. The integral response time is $\tau = \tau_0$ for a zero absorbing crystal. For nonzero absorption the integral response time τ can be measured experimentally and the corresponding τ_0 can be calculated for a given absorbance of the crystal from

$$\tau_0 = \frac{\tau\,\alpha d}{\exp(\alpha d) - 1}. \quad (12)$$

The thick lines in Fig. 11 represent calculations for $\alpha d = 2$ and $\tau_0 = 0.25$ s, which corresponds to $\tau = 0.8$ s with this absorbance. The relative weight of the high frequencies in the amplification spectra $\gamma'(\omega)/\gamma_0$ is much stronger in the case of an absorbing crystal and a relatively small broadening of the group velocity spectrum is revealed. Such transformation of the spectra may be important for a short pulse excitation like a δ pulse that generates a white spectrum in the system. This broadening can explain more complicated temporal profiles of the transmitted beam intensity $I_4(d,t)$ Correspondingly, the sharp jumps in the experimental dependences of the transmitted pulse delay [Figs. 6(a) and 9(a)] and of the half-width [Fig. 6(b)] on the input pulse half-width can be explained by a richer spectrum of the output signal.

It should be noted that the above discussion considers the two-beam coupling but a similar situation is present for BWFWM with a pump ratio r tending to zero. In both cases the intensity distribution in the crystal is mainly determined by the strong pump I_1, which is attenuated because of the absorption, and the transmittance spectrum of $I_4(d)$ in BWFWM is close to Lorentzian for zero absorption and relatively small coupling constants. Therefore the results of the analysis for the two-beam coupling configuration can be applied qualitatively for photorefractive BWFWM with these approximations. In spite of the fact that $\alpha d = 0.4$ is estimated for our crystal and that a smaller broadening of the bandwidth is expected, there are additional sources for a nonuniformity of the intensity, which also increase broadening. These are the recording by beams with Gaussian intensity distribution, the photorefractive scattering (beam fanning), and the corresponding depletion of the pumps, the imperfect overlapping of the beams. These additional factors act in a similar way as a larger absorption than plane waves recording in the medium with no beam fanning.

V. CONCLUSIONS

A slowing down of light pulses is achieved and studied with BWFWM in photorefractive crystals with different coupling constants. For short input pulses, the larger distortion of the transmitted output pulse $I_4(d,t)$ and the more complicated temporal profile in the crystal with the stronger coupling constant is explained by a more pronounced photorefractive self-enhancement effect. It is demonstrated that BWFWM ensures much larger delay of short pulses as compared to the two-beam coupling and guarantees the elimination of a precursor, which is a principal drawback for the slowing down of short pulses in the two-beam coupling approach. This feature can be used for optical signal processing when the delay of the leading edge of the pulse is important but the repetition rate is not crucial. For light pulses matching the bandwidth of the crystal the BWFWM scheme at small pump intensity ratio ensures almost the maximal delay, which can

be achieved in two-beam coupling with a given crystal. This small pump ratio is close to the optimal one for the crystals with a large coupling constant.

The photorefractive crystals we used in our experiments are quite slow at low intensities. The photorefractive response time is inversely proportional to the light intensity and varies from the 10^2 s range for ferroelectrics at low power excitation to the subnanosecond range for semiconductors at high-power pulsed excitation (see, e.g., [30]). Therefore the slowing down of pulses in the subnanosecond range may be achieved with fast photorefractive semiconductors. Moreover, the light pulses slowing down can be achieved with different BWFWM techniques. The slowing down characteristics, such as the dynamic range, the pulse delay and the nonlinear broadening, are determined by the response time of the medium, the type of the response (local or nonlocal), and the dispersive properties. That is why the dynamic range and characteristics of slowed down pulses in BWFWM scheme may be significantly extended.

ACKNOWLEDGMENTS

K. Shcherbin cordially thanks his colleagues from ICB for their help during his research stay at Université de Bourgogne. The authors are grateful to S. Odoulov and A. Shumelyuk for helpful discussions.

[1] A. Sommerfeld, Phys. Z. **8**, 841 (1907).
[2] L. Brillouin, *Wave Propagation and Group Velocity* (Academic Press, New York, 1960).
[3] A. Kasapi, M. Jain, G. Y. Yin, and S. E. Harris, Phys. Rev. Lett. **74**, 2447 (1995).
[4] L. V. Hau, S. E. Harris, Z. Dutton, and C. Behroozi, Nature **397**, 594 (1999).
[5] M. S. Bigelow, N. N. Lepeshkin, and R. W. Boyd, Science **301**, 200 (2003).
[6] P. Wu and D. V. G. L. N. Rao, Phys. Rev. Lett. **95**, 253601 (2005).
[7] K. Lee and N. M. Lawandy, Appl. Phys. Lett. **78**, 703 (2001).
[8] Y. Okawachi, M. S. Bigelow, J. E. Sharping, Z. Zhu, A. Schweinsberg, D. J. Gauthier, R. W. Boyd, and A. L. Gaeta, Phys. Rev. Lett. **94**, 153902 (2005).
[9] P.-C. Ku, F. Sedgwick, C. J. Chang-Hasnain, P. Palinginis, T. Li, H. Wang, S.-W. Chang, and S.-L. Chuang, Opt. Lett. **29**, 2291 (2004).
[10] S. Stepanov and M. P. Sánchez, Phys. Rev. A **80**, 053830 (2009).
[11] L. Thévenaz, Nature Photonics **2**, 474 (2008).
[12] E. Podivilov, B. Sturman, A. Shumelyuk, and S. Odoulov, Phys. Rev. Lett. **91**, 083902 (2003).
[13] G. Zhang, F. Bo, R. Dong, and J. Xu, Phys. Rev. Lett. **93**, 133903 (2004).
[14] S. Residori, U. Bortolozzo, and J. P. Huignard, Phys. Rev. Lett. **100**, 203603 (2008).
[15] B. Sturman, E. Podivilov, and M. Gorkunov, Appl. Phys. B **95**, 545 (2009).
[16] B. Sturman, P. Mathey, R. Rebhi, and H.-R. Jauslin, J. Opt. Soc. B **26**, 1949 (2009).
[17] P. Mathey, G. Gadret, and K. Shcherbin, Appl. Phys. B **102**, 539 (2011).
[18] R. W. Hellwarth, J. Opt. Soc. Am. **67**, 1 (1977).
[19] A. Yariv and D. M. Pepper, Opt. Lett. **1**, 16 (1977).
[20] D. M. Bloom and G. C. Bjorklund, Appl. Phys. Lett. **31**, 592 (1977).
[21] J. Feinberg and R. W. Hellwarth, Opt. Lett. **5**, 519 (1980).
[22] L. K. Lam, T. Y. Chang, J. Feinberg, and R. W. Hellwarth, Opt. Lett. **6**, 475 (1981).
[23] K. R. MacDonald and J. Feinberg, Phys. Rev. Lett. **55**, 821 (1985).
[24] O. Shumelyuk, A. Hryhorashchuk, and S. Odoulov, Ukr. J. Phys. **54**, 33 (2009). Available online at [http://www.ujp.bitp.kiev.ua/files/file/papers/54/1-2/540106p.pdf].
[25] K. R. MacDonald and J. Feinberg, J. Opt. Soc. Am. **73**, 548 (1983).
[26] M. Jeganathan, M. C. Bashaw, and L. Hesselink, J. Opt. Soc. Am. B **12**, 1370 (1983).
[27] B. I. Sturman, E. V. Podivilov and M. V. Gorkunov, Phys. Rev. A **77**, 063808 (2008).
[28] G. Brost, J. Norman, S. Odoulov, K. Shcherbin, A. Shumelyuk, and V. Taranov, J. Opt. Soc. Am. B **15**, 2083 (1998).
[29] G. Zhang, F. Bo, and J. Xu, *Photorefractive Materials and their Applications*, Springer Series in Optical Sciences, Vol. 115, edited by P. Günter and J.-P. Huignard (Springer Science+ Business Media, Inc., New York, 2007), pp. 277–294.
[30] K. Jarasiunas, J. Vaitkus, P. Delaye, and G. Roosen, Opt. Lett. **19**, 1946 (1994).